Metal-organic framework-intercalated graphene oxide nanofiltration membranes for enhanced treatment of wastewater effluents

Xinxin Chen [a], Vittorio Boffa [a],[*], Elisa Gaggero [b], Fanpeng Meng [d], Riccardo Navone [e], Daming Sun [a], Paola Calza [b], Murat Nulati Yesibolati [c], Peter Kjær Kristensen [f], Yuanzheng Yue [a]

[a] Department of Chemistry and Bioscience, Aalborg University, Fredrik Bajers Vej 7H, 9220 Aalborg, Denmark
[b] Dipartimento di Chimica, Universitá di Torino, Via Pietro Giuria 7, 10125 Torino, Italy
[c] DTU Nanolab - National Center for Nanofabrication and Characterization, Technical University of Denmark, DK-2800 Kongens Lyngby, Denmark
[d] Shandong Guiyuan Advanced Ceramic Co., Ltd (Sicer), Zibo, Shandong Province, China
[e] Publication Distribuzione s.r.l., Via Colonnello Archimede Costadura 2C, 73100 Lecce, Italy
[f] Department of Materials and Production, Aalborg University, Fredrik Bajers Vej 7H, 9220 Aalborg, Denmark

ARTICLE INFO

ABSTRACT

Graphene oxide membranes (GO) hold immense potential in the field of water purification. However, when applied directly to real wastewater effluents, pure GO membranes suffer from drawbacks such as fouling sensitivity and limited stability. To address these challenges and unlock the full potential of GO membranes, novel nanocomposite membranes have been developed by the intercalation of GO with nanoparticles of ZIF-8 (a type of zeolitic imidazolate framework). The prepared GO/ZIF-8 (GZ) nanocomposite membranes have exhibited enhanced hydrophilicity and exceptional water purification capabilities. Specifically, the GZ membranes have demonstrated a permeance enhancement of over two-fold when compared to the pristine GO reference membrane. This enhancement is coupled with anti-fouling performance and competitive rejection rates for both salts and organic pollutants. GZ membranes have been effectively employed for the purification by cross-flow filtration of 3 industrial wastewater effluents. They have shown improved separation performance compared to the pristine GO reference membrane, and high stability under cross-flow conditions. The origin of the high performances of the GZ membrane has been clarified using structural and morphological analyses. This work highlights the significant progress made in the field of water treatment using graphene-based membranes.

1. Introduction

Water, being one of the most vital resources on our planet, demands our utmost attention in terms of preservation and availability. Preserving water resources and ensuring water availability is crucial for human health and industrial development. The quality of water can be affected by a range of factors, including natural pollutants, industrial effluents, urban wastewaters, and agricultural runoff [1]. Consequently, there is a growing need for effective water purification technologies that can remove harmful contaminants from wastewater streams, enhancing the quality of water for human consumption, agricultural practices, and industrial processes. In this regard, membrane-based technologies have emerged as a promising approach to water treatment [2,3]. Among these technologies, nanofiltration (NF) has garnered attention as it demonstrates great potential for water purification [4,5] by removing organic pollutants and potentially toxic elements from water, while partially retaining the dissolved salts, which is often desirable in water potabilization [6], wastewater polishing [7], and in Zero-Liquid Discharge (ZLD) systems [8].

Several nanomaterials have been applied for the development of NF membranes with improved permeability, selectivity, stability, and antifouling properties [9]. Graphene oxide (GO) is a 2D carbon-based material, which is obtained by the oxidation of graphene, introducing oxygen-containing functional groups such as hydroxyl, epoxy, and carboxyl groups onto its surface, endowing GO with good hydrophilicity [10–12]. Therefore, GO is highly dispersible in water and can be easily processed to produce films, coatings, and composites for a broad range of applications, among which is membrane filtration [13]. Indeed, GO membranes have emerged as promising candidates for water purification due to their unique properties, which include exceptional water

permeability, tunable selectivity, and easy fabrication and functionalization [14–17]. However, the nanocapillaries between GO sheets have the tendency to expand in a wet environment, at the detriment of the membrane selectivity, and eventually causing the exfoliation and washing out of the membrane active layer under cross-flow filtration conditions [18]. Improvement of mechanical stability of GO membranes has been achieved by means of ionic, molecular, and nanoparticle crosslinkers [19]. This approach is interesting for application in water purification technologies because introduces the fascinating possibility to control the selectivity of GO membranes by tuning the space in between adjacent GO sheets.

Metal-organic frameworks (MOFs) are an emerging class of materials that consist of metal ions coordinated to organic ligands, creating a network of interconnected channels or pores. The combination of specific metal nodes and organic ligands allows for precise control over nanopore structure, morphology, and chemical functionalities of MOFs, thus providing advanced functional materials for a broad range of potential applications [20–22]. Molecular dynamic simulations have shown that MOF nanoparticles (e.g., Cu-BTC [23] and MIL-140A [24]) can be synergistically applied to fabricate nanocomposite GO membranes with enhanced stability and water permeability at optimal MOF loadings. Moreover, MOF nanoparticles can transfer new functionalities to the GO membranes, such as enhanced water permeability [25], oil-repellence [26], antifouling [27], and photocatalytic [27] properties. A few successful examples of MOF/GO nanocomposite membranes have been recently reported [24–29]. Nevertheless, these membranes were fabricated using filtration-based self-assembling methods, which questionably can achieve uniform and defect-free active layers over large areas. The enhanced performances of the final membranes were demonstrated only with model water systems (e.g., dye solutions) and often under filtration conditions far from the real life nanofiltration (e. g., in dead-end or vacuum filtration equipment).

In this work, we report the fabrication of novel MOF-intercalated GO membranes by the simple and scalable deposition method schematized in Fig. 1. The method involves a single-step spiral bar (Mayer rod) coating technique. The new MOF-intercalated GO membranes were applied to filter three real wastewater effluents, with the aim of providing experimental evidence of their industrial potential. Among the great variety of MOF materials, we selected ZIF-8 (zeolitic imidazolate framework-8) nanoparticles for GO intercalation, due to the unique molecular sieve structure and appropriate windows size (0.34 nm in diameter) [30,31]. Positively charged ZIF-8 nanoparticles strongly interact with the oxygen-containing functional groups of GO (e. g., carboxylic acids) thus providing mechanical stability to the membrane active layer under cross-flow filtration conditions. Moreover, the intercalation of GO by ZIF–8 can increase the interlayer spacing between GO sheets, thus facilitating water permeation through the membrane. Indeed, water molecules can access multiple permeation paths, which include the 3D porous structure of ZIF-8 and GO nanochannels. At the same time, GO sheets cover defects between ZIF-8 nanocrystals, thus providing a membrane that can combine high selectivity with good water permeability. Moreover, we added a humic acid substance (HA) as a crosslinker to stabilize the GO layered structure during cross-flow filtration. Indeed, in our previous works [32,33], we have demonstrated that humic-acid substances can establish ester bonds with the oxygen functional groups of graphene oxide oxygen functional groups, such as carboxylic acids and phenols, thus acting as a covalent crosslinker for the stabilization of the layered membrane structure.

1.1. Wastewater purification

In this study, the ZIF-8-intercalated GO (GZ) membranes were tested in a cross-flow filtration unit with samples of industrial wastewaters corresponding to emerging applications for NF membranes, namely a wastewater treatment plant effluent (WWTP-E), water from a recirculated aquaculture system (W-RAS), and water from the washing of industrial water-based flexographic printers (W-IFP). Filtration tests with these three real wastewater samples allowed for determining the optimal ZIF-8 loading, comparing the performances of the new membranes with the commercial ones, and checking their stability in the testing conditions. Hence, these tests permitted to foresee the potential of the GZ membranes in three relevant fields of application.
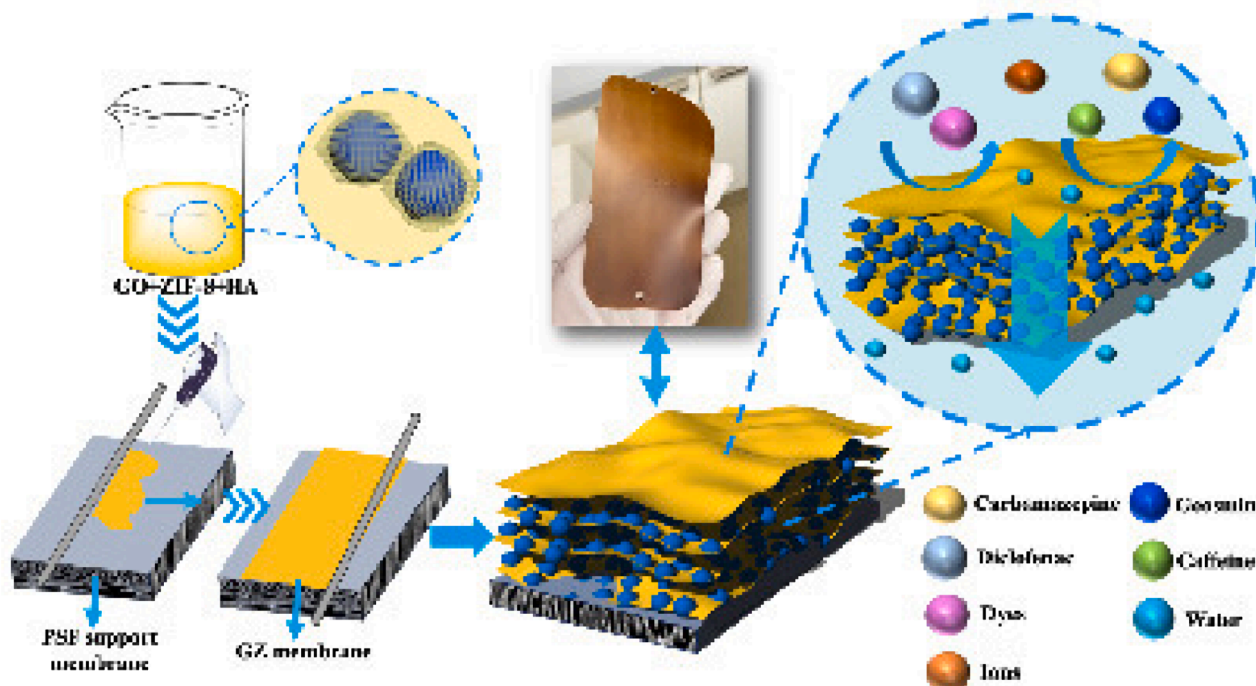

Fig. 1. Illustration of the procedure used for the fabrication of GO/ZIF-8 (GZ) intercalated nanofiltration membranes on a polysulfone (PSF) support in this study.

2. Experimental

2.1. Chemicals and materials

Polyethersulfone membrane (PSF, molecular weight cutoff, 25000 Da) was purchased from Alfa Laval. The graphene oxide (GO) used in this study was purchased from LayerOne Advanced Materials (Norway) as 10 wt% aqueous paste, consisting of layered GO sheets with lateral dimensions of several micrometers (Fig. S3). All the other chemicals were purchased from Sigma-Aldrich unless specified otherwise: zinc nitrate hexahydrate ($Zn(NO_3)_2·6H_2O$, purity $\geq$ 99 %), 2-methylimidazole (hereinafter named 2MI, 99 %), methanol (99.8 %), ethanol (absolute), HCl (37 %), NaOH (99 %), humic acid sodium salt (hereinafter named HA, technical grade), Geosmin ($\geq$97 %), NaCl (99 %, purchased from Chemsolute, Roskilde, Denmark), Na_2SO_4 (>99.0 %), $MgSO_4·7H_2O$ (99.0 % purchased from Acros Organics, Geel, Belgium).

2.2. Membrane synthesis

2.2.1. ZIF-8 synthesis

ZIF-8 nanoparticles were synthesized following the method proposed by Venna et al [34]. A mixture of Zn $(NO_3)_2·6H_2O$, 2-MI, and methanol (Zn/2-MI/methanol molar ratio = 1/8/243) was vigorously stirred for 40 min to facilitate the formation of ZIF-8 nanoparticles. Subsequently, the dispersion was subjected to centrifugation at 20,000 revolutions per minute (r.p.m.) for 10 min. The collected nanoparticles were then washed with ethanol. The centrifugation-washing procedure was repeated three times to ensure the removal of any impurities. Finally, the obtained ZIF-8 nanoparticles were dried overnight at 75 °C and stored until further use in the membrane coating process.

2.2.2. Preparation of the coating dispersions

GO was sonicated in Mili-Q (134 g L^{-1}) water for 10 min, followed by stirring for at least 1 h. Similarly, a HA solution (134 g L^{-1}) was sonicated in Mili-Q water for 10 min, followed by stirring for 4 h. The GO dispersion and HA solution were then combined to achieve a GO/HA weight-to-weight ratio of 60/40. 20 μL of HCl was added to 100 mL of the dispersion to promote condensation reactions between the functional groups in GO and HA [32]. The resulting solution was magnetically for 2 h. Subsequently, different amounts of ZIF-8 powder were introduced into the GO-HA dispersion, maintaining GO and ZIF-8 ratios of 9:1, 7:3, 5:5, 3:7, and 1:9 respectively. The resulting dispersion was subjected to sonication for 15 min and then stirred with a magnet for 6 h to ensure a high level of homogeneity before being used for membrane coating.

2.2.3. Membrane deposition

The PSF supports were first flushed with deionized water and then immersed in NaOH (a 1.0 g L^{-1}) solution for 1 h. Following this, the membranes were rinsed with the deionized water until the washing bath reached a natural pH. Finally, they were dried at room temperature and used for membrane coating. The nanofiltration (NF) membranes were prepared by casting the coating dispersion on the substrate via a spiral bar-coater 50 μm (TQC Ltd, Nottingham, UK). The membranes were then dried in air overnight and in a vacuum oven at 75 °C for 5 h. For ease of reference, the membranes were designated as GZ9-1, GZ7-3, GZ5-5, GZ3-7, and GZ1-9, based on the respective GO and ZIF-8 weight ratios of 9:1, 7:3, 5:5, 3:7, and 1:9.

2.3. Membrane characterization

XRD measurements were performed on an Empyrean XRD machine (Malvern Panalytical) with a monochromator Cu Kα radiation (1.5406 Å). Diffractograms were acquired in the *2θ* range from 5° to 25°, operating at 40 kV with a scanning speed of 8 min^{-1}. X-ray photoelectron spectroscopy (XPS) measurements were performed using a Specs XR50

with a non-monochromated Al Kα (1487 eV) X-ray source and a Phobos 1501D-DLD electron detector. Fourier transform infrared (FTIR) spectroscopy was carried out on Bruker TENSOR II equipped with a Bruker Platinum Attenuated Total Reflectance (ATR) attachment. The measurements were performed in the range of 4000–500 cm^{-1} by accumulating 64 consecutive scans. The acquired spectra were subsequently processed using the OPUS software. Zeta potential measurements were carried out using a powder dispersion by dynamic light scattering with a Zetasizer Nano-ZS (Malvern, UK). Scanning electron microscopy (SEM, ThermoFisher AFEG 250 Analytical ESEM) was employed to investigate the membrane surface and cross-section morphologies and to measure the thicknesses of the membranes. Membrane roughness was measured on a nGauge (ICSPI, ON Canada) Atomic Force Microscope (AFM). Dynamic water contact angle measurement was performed on an Attension Theta Lite (Biolin Scientific). Distilled water was dropped onto the membrane surface while the built-in camera took pictures every 0.05 s. The water contact angle (WCA) was determined for each membrane on the picture taken after 1.0 s the water drop (5 μL) touched the surface.

2.4. Filtration tests

The membranes were tested with pure water, model salt solutions (1 g L^{-1} of NaCl, Na_2SO_4, and $MgSO_4$ in deionized water), and real wastewater samples, i.e., WWTP-E that was collected at a Danish wastewater treatment plant, W-RAS which was provided by a trout farm, and W-IFP which was provided by Publication Distribuzione s.r.L. (Lecce, Italy). Filtration tests were performed on the lab-made equipment, which is described elsewhere [35] at a transmembrane pressure of 6 bar and crossflow velocity of about 2 m s^{-1}. Membrane rejections (*R%*) were calculated based on the equation R% = $(1 - C_p/C_f) \times 100$, where C_f and C_p are the concentrations of the target species in the feed and permeate, respectively. Single salt concentrations were determined by measuring the electrical conductivity with a Seven Multi (Mettler Toledo, Columbus, OH, USA). Total Organic Carbon (TOC) was measured by using a TOC-VCSH analyzer. Real wastewater effluents were sparked with the relevant organic pollutants which are listed in Table1 (carbamazepine (5 mg L^{-1}), caffeine (5 mg L^{-1}), diclofenac (5 mg L^{-1}), and geosmin (500 ng L^{-1})) to facilitate water analyses and therefore have a good assessment of the membrane selectivity for water contaminants.

Membrane feed and permeate samples collected during the WWTP-E filtration tests were analyzed with a Merck-Hitachi HPLC system equipped with an L-6200A Intelligent Pump, an L-4200 UV–VIS Detector, and a six-way Rheodyne valve injection system. The detection wavelength was set at 285 nm for caffeine and carbamazepine and at 220 nm for diclofenac. Elution was performed with a mixture of phosphoric acid solution at pH 2.8 (A) and acetonitrile (B) at a flow rate of 1 mL min^{-1} in the following condition: 25 % B and 75 % A for caffeine (retention time = 1.75 min.) and carbamazepine (retention time = 5.55 min.), 65 % B and 35 % A for diclofenac (retention time = 3.13 min.). The W-RAS sample was sparked with geosmin (Table 1) and the concentration of this off-flavor compound in the feed and permeate samples collected during filtration was tested as follows: water samples were concentrated by using a solid phase microextraction syringe fiber (SPME) [36]. Gas chromatography-mass spectrometry (GC–MS, 8860 system coupled with a 5977B MS detector, Agilent, USA) was developed for the analysis of the geosmin, as described elsewhere [36].
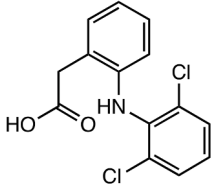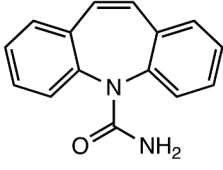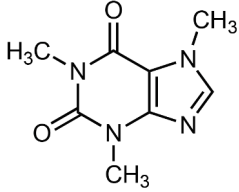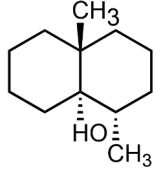
3. Results and discussion

3.1. GZ nanocomposites

The ZIF-8 nanoparticles were successfully synthesized and characterized by SEM, revealing a polyhedral structure with a uniform size of about 130 nm, as shown in Fig. 2a. Furthermore, Fig. 2b displays the micrograph of a pure GO membrane specimen exhibiting a layered

Table 1

Model pollutants investigated in this study and their molecular properties, as obtained from literature [37,38] *LogD is here reported for diclofenac, which is negatively charged at pH = 7.

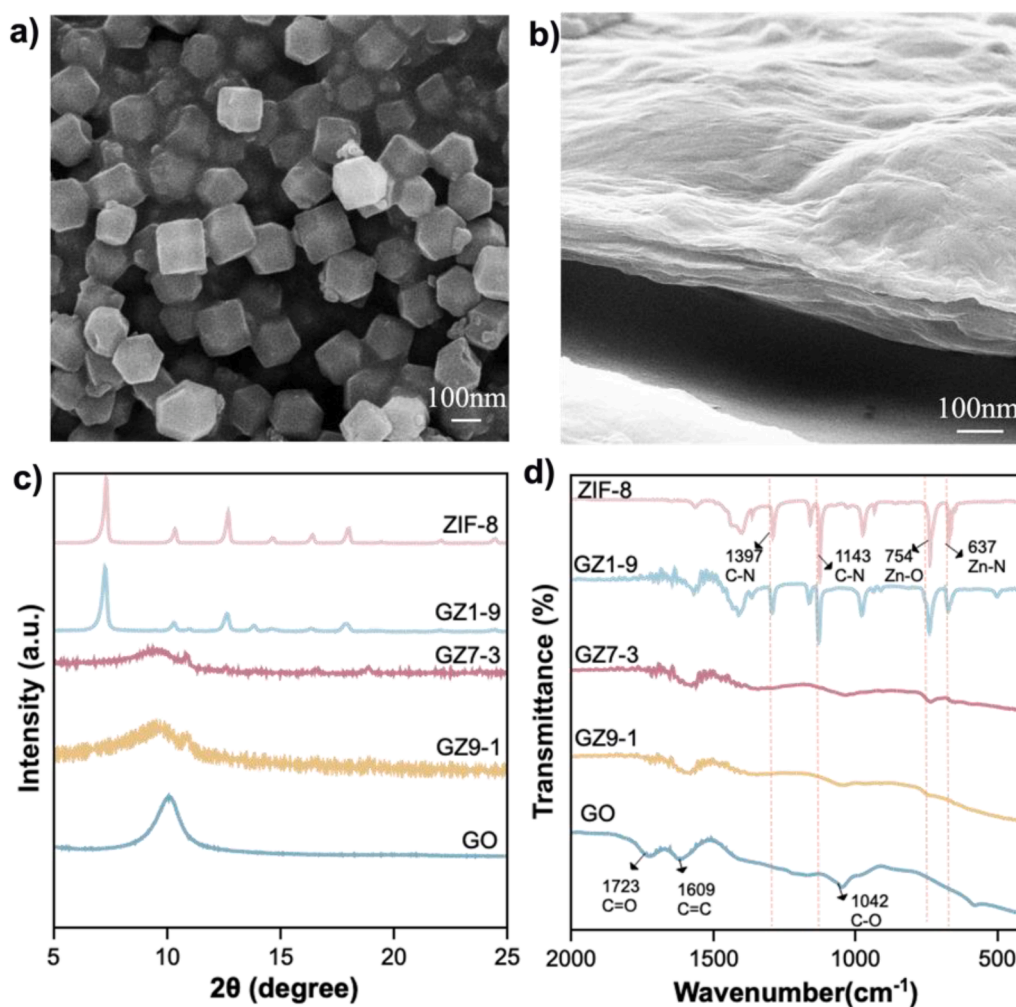| Effluent	WWTP-E			W-RAS
Target pollutants	diclofenac	Carbamazepine	caffeine	geosmin
Chemical structure				
Category	analgesic drug	antiepileptic drug	psychoactive drug	off-flavor compound
Molecular weight (g·mol^{-1})	296.15	236.27	194.19	182.31
LogP; *LogD	1.77*	1.895	−0.628	3.13

Fig. 2. (a) SEM image of ZIF-8 nanoparticles; (b) SEM image of a self-standing GO membrane; (c) XRD patterns of GZ composite nanofiltration membranes; (d) FTIR spectra of the GZ composite nanofiltration membranes. The positions of the ZIF-8 characteristic peaks in the starting MOF powder and GZ nanocomposites are indicated by vertical dotted lines.

structure and a smooth surface with minor wrinkles. In order to verify the intercalation of ZIF-8 into GO, the interlayer spacing between GO nanosheets in the GZ composite nanofiltration membrane was analyzed using XRD, and the corresponding results are presented in Fig. 2c. The ZIF-8 diffractogram clearly exhibits the characteristic reflections of this MOF material, centered at *2θ* of 7.3°, 10.4°, 12.7°, which align with the literature data [34]. The intensity of these reflections decreases as the concentration of GO in the material increases. The characteristic diffraction of GO is centered at *2θ* of 10.1°, corresponding to an interlayer spacing of 0.87 nm, as calculated using the Bragg equation. This interlayer spacing is typical for GO membranes [39] and is consistent with their selectivity in the nanofiltration range. The addition of ZIF-8 nanoparticles significantly leads to a noticeable shift in the characteristic peaks of GO towards lower angles. In particular, the composite

nanofiltration membranes GZ9-1 and GZ7-3 exhibits a diffraction peak at 9.6°, corresponding to an interlayer spacing distance of 0.93 nm. The increased interlayer spacing is a direct result of ZIF-8 intercalation between the GO layers. However, as the loading of ZIF-8 nanoparticles continued to increase, the GZ composite nanofiltration membrane did not show any diffraction peak attributable to the staking of the GO sheet, which is a result of the complete intercalation with ZIF-8 nanoparticles.

To further demonstrate the efficient intercalation of ZIF-8 with the GO, the functional groups on the membrane surface were analyzed using FTIR, as is shown in Fig. 2d. The spectrum of GO exhibited a broad band at 3338 cm^{-1}, corresponding to the strong stretching mode of OH group, as well as absorption peaks at 1609 cm^{-1} and 1723 cm^{-1}, attributed to the C=C stretching mode and C=O, respectively. In comparison to pristine GO, the FTIR spectra of GZ nanocomposites did not show a peak at 1723 cm^{-1} (C=O stretching). Additional bands observed at 1143 cm^{-1} and 1397 cm^{-1}, corresponding to C-N bonds in the imidazole group, 754 cm^{-1} for Zn–O bonds, and 637 cm^{-1} for Zn-N bonds, were attributed to the ZIF-8 structure [40–42]. All the membranes (GZ9-1, GZ7-3, GZ5-5, GZ3-7, GZ1-9) exhibited the presence of bonds corresponding to both GO and ZIF-8, which further confirmed the formation of the targeted GZ nanocomposites. Moreover, the X-ray photoelectron spectroscopy (XPS) analysis (Fig. S1A) revealed that the N and Zn atomic concentrations in the GZ nanocomposites increased with the ZIF-8 loading. Conversely, the pure GO membrane exhibits no signals for Zn and N elements. The high-resolution spectra of Zn $2p$ electrons can be fitted with two peaks with binding energies of 1022 eV and 1044 eV (Fig. S1D, G, and J), as already reported for ZIF-8/GO membranes in the literature [43]. The C 1 s peaks (Fig. S1B) of the GO membrane could be deconvoluted in three peaks centered at 284.8 eV, 286.6 eV, and 287.6 eV, corresponding to carbon atoms with an increasing degree of oxidation, as typical for GO materials [43–45]. The relative intensities of these peaks change upon the addition of the imidazole carbon in the GZ composites. Moreover, the O 1 s characteristic peaks of the GO oxygen functions (Fig. S1C) centered at 530.1 eV (C=O) and 531.9 eV (O-C=O/C-O-C) shifted towards progressively higher binding energies by increasing the ZIF-8 loading in the GZ composites. Indeed, the GZ9-1 (Fig. S1F), GZ7-3 (Fig. S1I), and GZ5-5 (Fig. S1L) presented the C=O signal centered at 530.7 eV,531.0 eV, and 531.5 eV respectively, and the O-C=O/C-O-C signal at 532.3 eV, 532.4 eV, and 532.8 eV respectively, indicating that 2-methylimidazole can form hydrogen bonds with the oxygen functional groups in GO (Fig. S1B–E). Based on the literature [43], the formation of such hydrogen bonds can reduce the interface gap between GO sheets and ZIF-8 crystals, thus increasing the sieving function of the membrane.

3.2. Morphology and surface properties of GZ membranes

Fig. 3 displays SEM micrographs of the surfaces and cross-sections of GZ nanocomposite nanofiltration membranes fabricated with different loadings of ZIF-8 nanoparticles. The pure GO membrane, without ZIF-8 nanoparticles, exhibited a remarkably smooth and continuous surface with subtle wrinkles, consistent with the micrograph of the unsupported material in Fig. 2b. The cross-section of the GO active layer has a thickness of 0.54 μm and appears homogenous and compact, owing to the two-dimensional layered structure of GO [46]. The deposition of ZIF-8 on the GZ composite membranes was confirmed by the concentrations of zinc and nitrogen atoms detected by EDX analysis (Fig. S2E). Furthermore, the EDX mapping showed that C, O, N, and Zn indicate that the ZIF-8 nanocrystals are uniformly dispersed in the composite membranes (Fig. S2A–D). A noticeable increase in membrane thickness can be observed, as the loading of ZIF-8 nanoparticles goes from 0 to 50 wt%: 1.25 μm (GZ9-1), 1.97 μm (GZ7-3), and 1.98 μm (GZ5-5). The total solid content of the coating dispersions used for GZ membrane preparation is constant. Therefore, the increase in membrane thickness can be ascribed to the intercalation of the 3D ZIF-8 nanocrystals between the 2D GO sheets which leads to an expansion of the space between GO
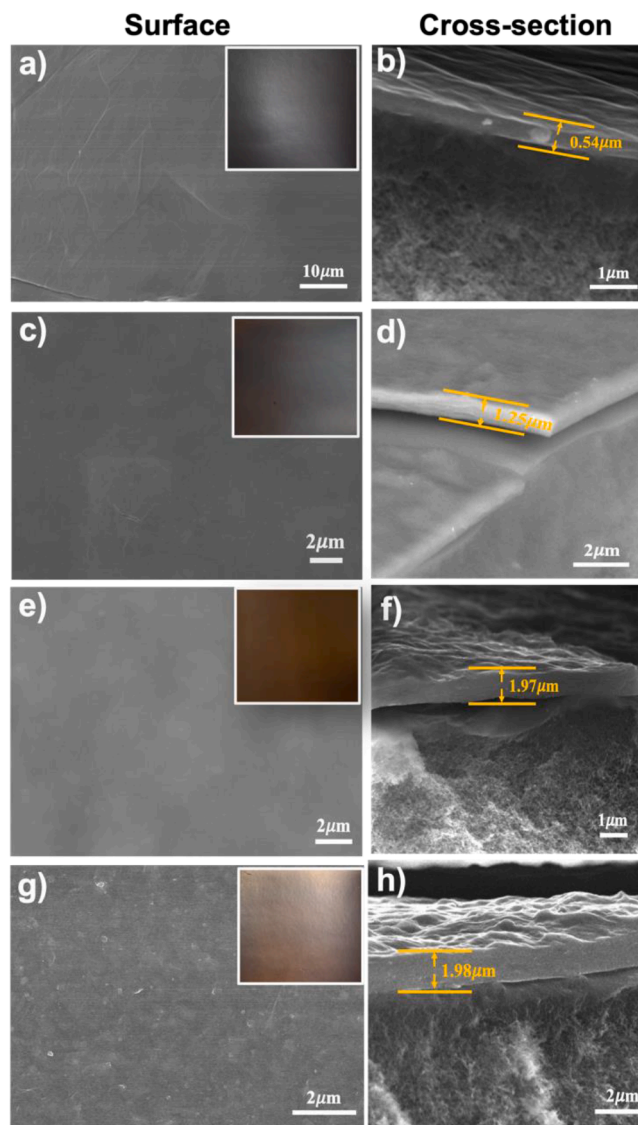

Fig. 3. SEM micrographs of the surfaces and cross-sections of different nanocomposite membranes, namely GO(a-b); GZ9-1(c-d); (c) GZ7-3(e-f); (d) GZ5-5 (g-h). Pictures of the membrane surfaces are reported in the inserts of the corresponding micrographs.

layers, which is here expected to facilitate water permeation. However, the incorporation of the ZIF-8 nanoparticles in the GO matrix also caused an increase in the roughness of the membrane surface. Moreover, when the ZIF-8 loading reached 50 wt%, the membrane exhibited granular bulges, which can be ascribed to aggregates of nanocrystals. Due to the presence of these aggregates, it was not possible to achieve continuous GZ active layers for ZIF-8 loadings ≥ 70 wt%.

Surface properties, such as hydrophilicity and charge, produce a relevant impact on the permeability and selectivity of nanofiltration membranes. Therefore, the influence of ZIF-8 nanocrystals on the characteristics of the surface of the GZ membranes was assessed through surface roughness, water contact angle, and ς–potential measurements. The average surface roughness (Ra) was attained from the AFM depth profile of the coated membranes, which are shown in Fig. 4. In general, as already observed at SEM, the ZIF-8 nanoparticles can induce wrinkling and form aggregates on the membrane surface, leading to an increased surface roughness compared to the GO reference membrane (Ra = 49.9 nm). Loadings of ZIF-8 nanoparticles ≤ 30 wt% cause only a moderate change in the active-layer roughness, as observed in the GZ9-1 and GZ7-3 membranes with Ra values of 56.8 nm and 57.5 nm,
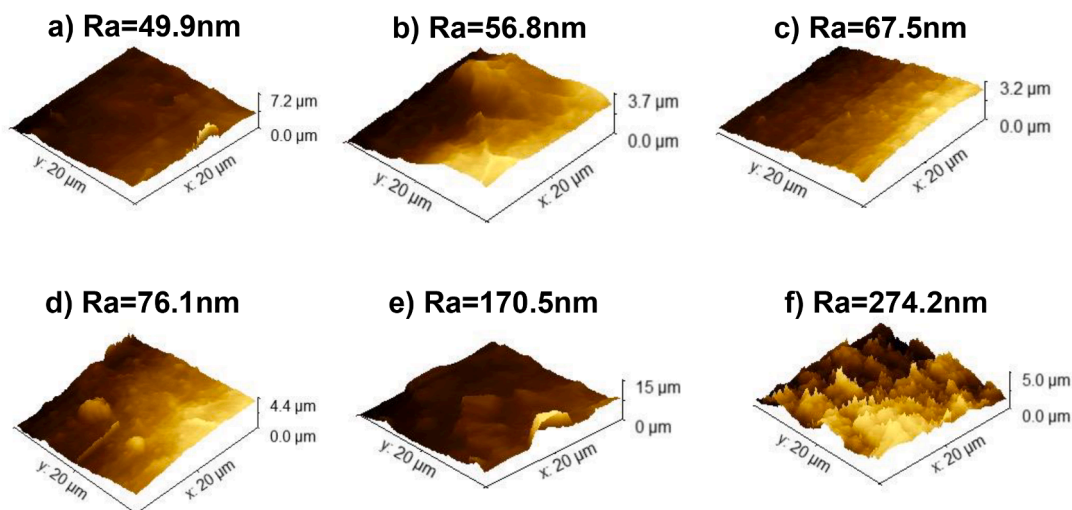
Fig. 4. AFM images of GO and GZ membranes: (a) GO; (b) GZ9-1; (c) GZ7-3; (d) GZ5-5; (e) GZ3-7; (f) GZ1-9.

respectively. On the contrary, for loadings of ZIF-8 nanoparticles of 50 wt% or higher, the formation of nanoclusters on the membrane surface leads to a progressive increase of *Ra*: from 76.1 nm (GZ5-5) to 170.5 nm (GZ3-7), and 274.2 nm (GZ1-9). GZ3-7 and GZ1-9 present not only big roughness but also low adhesion on the substrate, resulting in highly defective membranes.

It has been previously reported that hydrophilicity plays a pivotal role in the purification of water by NF membranes, as it facilitates enhanced water permeability and mitigates fouling, ensuring efficient and sustainable filtration processes [47,48]. The surface hydrophilicity of the GZ composite nanofiltration membrane was assessed by measuring the water contact angle (WCA) and the results are displayed in Fig. 5a. The WCA of the PSF support after the activation procedure (as mentioned in 2.2.3) was 46.7°±2, indicating a moderate hydrophilic surface. Surface hydrophilicity was increased after coating the GO active layer (WCA = 33.3°±3), which presents a relatively smooth surface and a large number of surface oxygen-containing functional groups, namely hydroxyls, carboxylic acids, and epoxy, which can strongly interact with water molecules, e.g, by hydrogen bonding. On the contrary, the ZIF-8 framework is inherently hydrophobic since the imidazole linkers do not contain hydrophilic functional groups [49]. Nevertheless, when the loading of ZIF-8 nanoparticles was below 30 wt%, WCA gradually

decreased to reach $25 \pm 2°$ and $20 \pm 2°$ for GZ9-1 and GZ7-3, respectively. However, by increasing the ZIF-8 loading from 50 wt% to 90 wt%, WCA progressively increased from $23 \pm 2°$ (GZ5-5) to $33 \pm 1°$ (GZ3-7), and $40 \pm 3°$ (GZ1-9). To explain this V-shaped trend, we shall consider both the hydrophilicity of the ideally smooth GZ surfaces (here calculated according to the Wenzel model and reported in Fig. S4) and the surface roughness of the membrane active layers. Indeed, Fig. S4 shows that ZIF-8 loadings ≤ 30 wt% produce no significant differences in the Wenzel contact angle compared to the GO reference membrane. Therefore, intercalations of small quantities of ZIF-8 in the GO layered structure increased the surface roughness and the exposure of hydrophilic surface functions in such a way as to reduce the measured WCA [50] of the GO-like surface. On the contrary, we observed progressively higher Wenzel contact angles by raising the ZIF-8 loading from 50 wt% to wt90 %, which can be explained by an increased exposure of the ZIF-8 nanoparticles at the membrane surface and is consistent with the increased observed WCA in Fig. 5a.

The surface charge of NF membranes plays a crucial role in determining their ion-transport selectivity, due to the electrostatic interactions with charged solutes [51]. Fig. 5b shows the ς-potential of the membrane materials as a function of ZIF-8 loading at pH values of 4.0, 7.0, and 10.0. As expected, the net GO presented a negative ς-potential
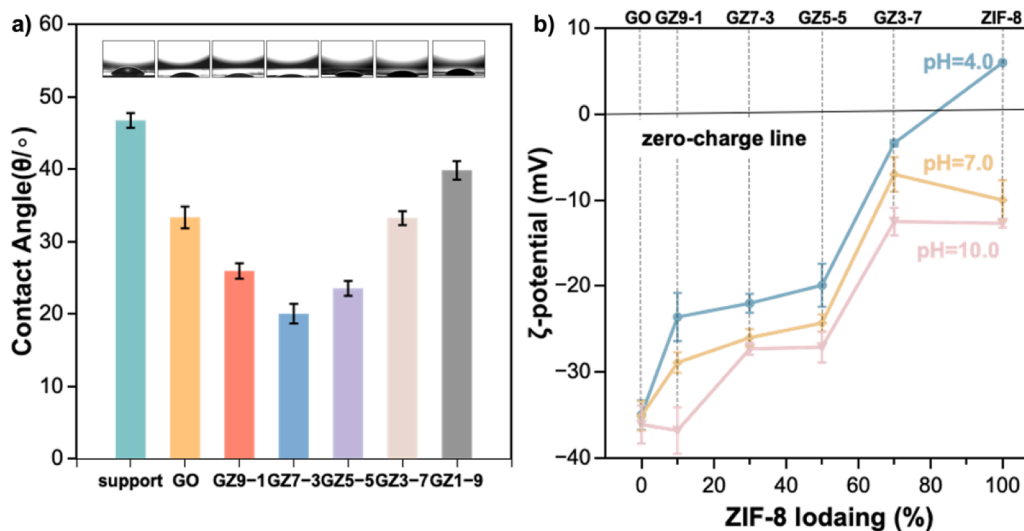

Fig. 5. (a) Water contact angle measurements for the support, GO, and membranes with different ZIF-8 loading. (b) Zeta potential variations of the membrane materials (GO, GZ9-1, GZ7-3, GZ5-5, GZ3-7, ZIF-8), as a function of the pH changes.

charge of about −40 mV over all the analyzed pH range [52,53], which is consistent with the oxygen functional groups, e.g., carboxylic acids. On the contrary, the ς-potential ZIF-8 nanocrystals decreased from −12.7 ± 0.2 mV at pH 10.0 to −10 ± 2.3 mV at pH 7.0, to reach the positive value of 6.0 ± 0.2 mV at pH 4.0, in agreement with literature data [54], which indicate that ZIF-8 nanoparticles have isoelectric point between pH 4.0 and pH 7.0. Like, GO, GZ materials with loadings ≤ 50 % presented a highly negative charge surface even at pH 4.0. This is coherent with nanocomposites in which the ZIF-8 nanocrystal is completely embedded and fully covered by the GO matrix. While, as already observed by SEM and WCA analyses, ZIF-8 loadings ≥ wt70 % result in nanoparticle aggregation and GZ materials exposing both GO and MOF moieties at the surface, which implies a lower density of negative charges on the surface for each of the tested pHs.

In conclusion, ZIF-8 intercalation increased the interlayer space between GO sheets and the hydrophilicity of the GO membrane surface. These features are potentially beneficial for the water permeability of the membrane's active layer. On the other hand, for ZIF-8 loadings higher than 50 wt%, nanoparticles in the coating dispersions formed aggregates, with a negative impact on the homogeneity of the membrane active layer, which presented naked eye-visible surface defects, preventing them from practical applications. For this reason, filtration tests were only performed with membranes prepared at ZIF-8 loadings ≤ 50 wt%.

3.3. Water desalting

First, we tested the newly developed GZ membranes by filtering demineralized water and model salt solutions. In general, we did not observe a significant difference in permeation rate while filtering water and salt solutions, consistently with the low salt concentration (1.0 g L^{-1}), high cross-flow velocity (2 m s^{-1}), and low recovery rate (10 %) achieved during these tests. The average permeances are reported in Fig. 6b for each membrane together with the standard deviations over 4 filtration tests performed on different specimens. The PSF support, here reported as a reference, exhibited a water permeance of 24 ± 2 L m^{-2} h^{-1} bar^{-1}, which was substantially reduced after membrane coating, suggesting the formation of continuous active layers. The GO showed water permeance of 1.9 ± 0.3 L m^{-2} h^{-1} bar^{-1}. ZIF-8 intercalation highly enhanced the water permeance of the GZ membranes, consistently with the widening of the GO interlayer space (Fig. 2) and the increased hydrophilicity (Fig. 5a) of the membranes. The water permeance increases by raising the ZIF-8 loading from 10 wt% to 50 wt%, and permeance values of 2.8 ± 0.1, 3.2 ± 0.1, and 3.5 ± 0.3 L m^{-2} h^{-1} bar^{-1} were measured for GZ9-1, GZ7-3, and GZ5-5, respectively. The permeation

and the selectivity of GO-based membranes depend on an interplay of factors, which include the degree of oxidation of the graphene sheets [55], type of the crosslinker used for the structural stabilization [56,57], and even the filtration *trans*-membrane pressure, which can cause compaction of the GO layers [58]. Indeed, a broad range of performances has been reported for GO membranes [59,60].

ZIF-8 and GO provide multiple permeation paths, which include the microporous network of the MOF and the interlayer nanochannels in the hydrated GO layered structure. ZIF-8 nanocrystals present an accessible pore window of 0.34 nm, which is suited to reject organic solutes and hydrated ions by size exclusion [38]. In this work, we stabilized the GO layered structure via covalent cross-linking with HA [40] and we measured an average nanochannel size of 0.87 nm for GO and 0.96 nm for GZ9-1 and GZ7-3, which is theoretically suited for the permeation of hydrated ions [61]. GZ membranes with ZIF-8 loading higher than 50 wt % disturbed the staking of GO layers and the formation of nanochannels, as revealed by the absence of any characteristic GO peak in the diffractograms of these materials. Hence the selectivity of the GZ membranes depends on the ZIF-8 loading and the interaction of ZIF-8 nanoparticles with GO sheet. The GZ membranes exhibited competitive NF rejections for NaCl, MgSO₄, and Na₂SO₄, as shown in Fig. 6b, and are therefore apt for rejecting sulfates and other multi-charged anions [62]. In general, GZ9-1 and GZ7-3 present higher salt rejections than the GO reference for all the tested salts. GZ7-3 achieved rejections of 58 %, 63 %, and 74 % for NaCl, MgSO₄, and Na₂SO₄, respectively. Such rejection rates are a consequence of the good interaction between the GO functional groups and the ZIF-8 microporous network (as indicated by the XPS analysis), which can provide a thigh structure in the hydrated state and narrow the non-selective defects between GO layers. Moreover, GZ materials showed enhanced water permeability (permeance × active layer thickness) compared to recently reported GO-based membranes (Fig. 6c) [63–65]. Some of these GO-membranes are fabricated, e.g. via layer-by-layer deposition [66] in Fig. 6c, as < 100 nm thin films allow for high water permeation rates, but their industrial fabrication is complex. On the contrary, our GZ membranes were prepared simply by a single coating of ZIF-8/GO dispersions. GZ membranes showed also good performances with respect to the permeance of the reported GO-based membranes in the literature. For instance, Endo et. al. [63] reported ultrathin GO/graphene/deoxycholate membranes with NaCl rejection of about 85 %, water permeance of 0.35 L m^{-2} h^{-1} bar^{-1}, that is one order of magnitude lower than those of our GZ membranes. On the other hand, An et al. [65] developed an ice-crystal templating approach for the fabrication of GO membranes with great water permeance (22.6 L m^{-2} h^{-1} bar^{-1}). Nevertheless, these membranes presented NaCl rejection < 20 %, which is much lower than the 58 ± 1.4 % observed for
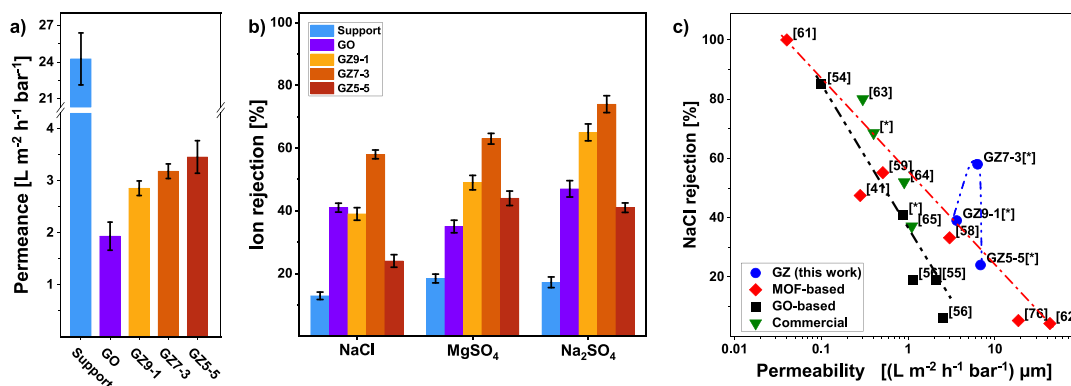

Fig. 6. Filtration performance of the PSF support and GZ membranes when filtering NaCl Na₂SO₄, and MgSO₄ model solutions (1.0 g L^{-1}): (a) permeance and (b) ion rejection. Section (c) provides a comparison of the performances of the GZ active layers with recently reported MOF-based membranes (ref. [31,41,62–65]), commercial polyamide NF membranes (ref. [67–68]), and recently reported GO-based membranes (ref. [59–61]). The red line and the black line indicate the water permeability – NaCl selectivity trade-off of MOF-based and GO-based membranes respectively. [*] Data collected in this study. (For interpretation of the references to colour in this figure legend, the reader is referred to the web version of this article.)

the GZ7-3 membrane. Additionally, the GZ7-3 membrane overcame the permeability-selectivity trade-off of the MOF-based water desalination membranes [35,45,70–73] and of the commercial NF90 [72] and NF270 membranes [61,74,75]. On the other hand, salts rejections noticeably decreased to 24 % for NaCl, 44 % for MgSO$_4$, and 41 % for Na$_2$SO$_4$ for GZ5-5, i.e., when the GZ membrane was prepared with a ZIF-8 loading of 50 wt%, following the partial aggregation of ZIF-8 nanoparticle and the consequent enlargement of the transport paths in the GZ active layer.

3.4. Depollution of real wastewater effluents

The filtration performances of the GZ composite membranes were evaluated for three different water sources: wastewater treatment plant effluent (WWTP-E), water from the recirculated aquaculture system (W-RAS) and washing water waste from an industrial printing company (W-IFP). Table 2 presents the characteristic parameters, including pH, conductivity, and total organic carbon (TOC), for the three water streams.

3.4.1. WWTP-E

An increasing number of organic pollutants are found in urban wastewater. These contaminants of emerging concerns (CECs), which include a wide range of synthetic chemicals, such as pharmaceuticals, personal care products, and endocrine-disrupting compounds, have traditionally not been monitored or regulated. Even if CECs are typically found in water at low concentrations (from ng L^{-1} to μg L^{-1}) they are increasingly recognized as a potential risk for the environment and human health [75]. The conventional physical and biological treatments are not effective in their abatement, thus requiring further polishing of WWTP-E. Here we investigated the permeability and the rejection of the GZ membranes to target CECs, namely carbamazepine, caffeine, and diclofenac to assess the potential of this technology as a tertiary treatment for WWTP-E. Compared to the model salt solutions, WWTP-E contained a consistent amount of non-toxic organic matter (mg L^{-1} level), which might have an impact on the membrane permeance and low concentrations of persistent organic pollutants, which might represent a potential treatment for aquatic ecosystems and human health. For this reason, we investigated the decline of permeate flux (Fig. 7a) together with the selectivity of the 3 target pollutants (Fig. 7b) while filtering WWTP–E. The initial permeate flux followed the order: GZ5-5 > GZ7-3 > GZ9-1 > GO, as already observed for the membrane permeances when filtering model solutions (Fig. 6a). Moreover, the permeate flux decreased during filtration, as expected when treating a real wastewater effluent due to the membrane fouling. The flux decline (-ΔJ) was more pronounced for the GO reference membrane (-3.8 ± 0.3 L m^{-2} h^{-1}), followed by GZ9-1 (-1.3 ± 0.3 L m^{-2} h^{-1}) and GZ7-3 (-1.0 ± 0.2 L m^{-2} h^{-1}), while the decline for GZ5-5 was negligible in the observed filtration time, which is consistent with the fact that membrane hydrophilicity increased with the ZIF-8 loading (Fig. 5a) thus hindering deposition of organic matter on the membrane surface. Moreover, all the membranes were selective to a certain extent towards the target organic pollutants investigated in this study. The rejection of the organic pollutant is expected to depend on size exclusion [11,61], although electrostatic repulsion can also play a role in the case of diclofenac. Moreover, the chemical affinity/disaffinity of the pollutants with the hydrophilic GZ material can either facilitate or hinder its adsorption and diffusion through the membrane layer [76]. As observed for salt rejections, GZ9-1 and GZ7-3 showed higher rejection of water

contaminants than the reference GO membrane, while GZ5-5 offered again poor selectivity. Among the tested contaminants, caffeine was the one with the lowest molecular weight and the most hydrophilic, as indicated in Table 1, and presented the lowest rejection values (Fig. 7b). Despite that, GZ9-1 and GZ7-3 reached rejections of 63 ± 2 % and 72 ± 2 %, respectively. Furthermore, GZ9-1 demonstrated excellent performance reaching rejections of 98 ± 2 % for diclofenac and 82 ± 2 % for carbamazepine, which have higher molecular mass and are more hydrophobic than caffeine. Moreover, both GZ9-1 and GZ7-3 presented superior rejections for the target pollutants, higher permeation rates, and enhanced fouling resistance compared to the GO reference membrane.

3.4.2. W-RAS

Recirculating aquaculture systems (RAS) are land-based facilities, which allow minimizing water consumption by the continuous treatment and recirculation of the water effluents from the fish tanks. A major issue for RAS is the accumulation of off-flavor compounds, such as geosmin and 2-methylisoborneol (2-MIB) [77], which are secondary metabolites of various microorganisms that are often present in aquaculture ecosystems and can be adsorbed by the lipid-rich tissues of fishes making their meat unmarketable [78]. In this context, NF has been proposed as an effective method for preventing the accumulation of these unwanted compounds in RAS by filtering a side stream of the fish tank effluent after the biological treatments [79]. Therefore, the new membranes were tested with a W-RAS from a rainbow trout farm for their rejection to geosmin.

Fig. 8 presents the results of the filtration tests with water from a recirculated trout farm loop. Water permeance (Fig. 8a) increased from 1.4 L m^{-2} h^{-1} bar^{-1} for the GO membrane to 3.8 L m^{-2} h^{-1} bar^{-1} for the GZ5-5 membrane, following the same trend observed for the WWTP-E. Moreover, all the tested membranes presented ~90 % rejection for geosmin, as depicted in Fig. 8b. Such a high rejection rate can be ascribed to the hydrophobic character of this off-flavor compound (log P = 3.13 as reported in Table 1), which limits adsorption on the membrane surface and diffusion across the hydrophilic nanochannels in the GZ composites layers. Remarkably, GZ membranes achieved superior rejection values than what was reported for the commercial NF90, which rejected 58.2 % of geosmin in treated water from Lake Tai in China [80] (permeance ~ 2 L m^{-2} h^{-1} bar^{-1}), and of other commercial NF membranes NF90, NF270, and NTR7450 when polishing water samples from the Palmer and Myponga potabilization plants in Australia [81]. The GO and GZ membranes also outperformed the lab-made alumina–zirconia NF membrane reported by Kang et. al. [82], which rejected 65 ± 2 % of the geosmin dissolved in a model solution (permeance 15 L m^{-2} h^{-1} bar^{-1}). Fig. 8c shows that the rejections of the dissolved ions and TOC in the complex W-RAS matrix followed the trend GZ3-7 > GZ1-9 > GO > GZ5-5, as observed for the model solutions reported in Fig. 6b. Specifically, ion rejections ranged between 66 % for GZ3-7 and 35 % for GZ5-5, while TOC rejections dropped from 68 % for GZ3-7 to 23 % for GZ5-5. This variability in the ion and TOC rejection performances of the GZ membranes, coupled with their great geosmin rejection, offers many opportunities for their applications in RAS, where the need to minimize the concentration of off-flavor compounds, such as geosmin, in the loop, shall no compromise the optimal concentration of salts and nutrients for the sake of fish well-being.

3.4.3. W-IFP

Within the current trend to replace traditional industrial formulations with green chemicals, an increasing number of water-based inks are used for industrial printing. However, a large volume of water is needed to wash the machines at the end of each printing cycle, thus producing a substantial amount of wastewater with code 080,308 according to the European Waste Catalogue [44], the disposal of which is costly. An integrated approach can be used to minimize the discharge of this liquid effluent while reusing the purified water for washing the

Table 2
Characteristic parameters of the wastewater effluents tested in this study.

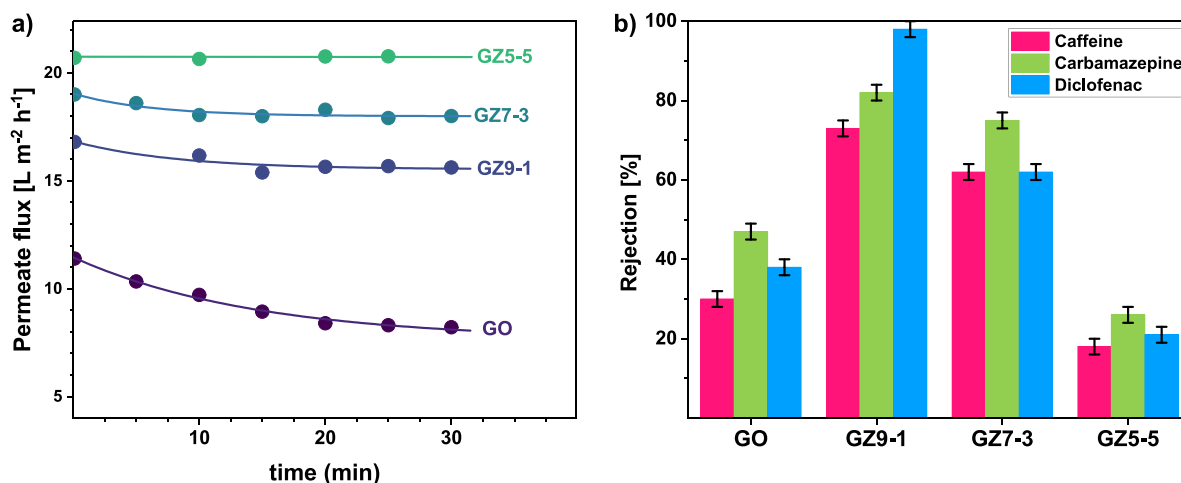| Type	pH	Conductivity (μS cm^{-1})	TOC (mg L^{-1})
WWTP-E	8.23	936.3	16.3
W-RAS	7.41	3062	18.7
W-IFP	7.62	1264	567

Fig. 7. Filtration of WWTP-E: (a) permeate fluxes as a function of the filtration time and (b) rejections of target pollutants. Error bars indicate the error in the determination of the pollutant rejections by HPLC analysis.
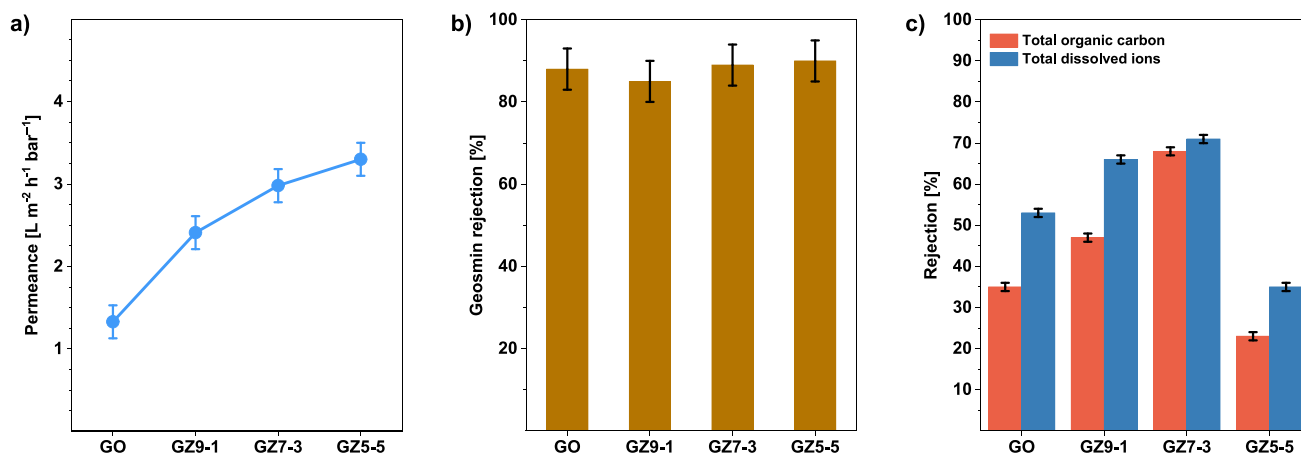

Fig. 8. Filtration of W-RAS over GZ membranes and the GO reference: (a) permeance (average values taken on different membrane specimens and at different filtration times), (b) geosmin rejection, (c) retention of the total organic carbon (TOC) and dissolved ions. Error bars indicate the errors in the determination of the geosmin by GC–MS, TOC, and conductivity analyses.

machines. Therefore, in this work a W-IFP is tested to show that the permeate of the GZ membranes can be used as a washing medium for industrial printers, thus simultaneously reducing water consumption, and minimizing wastewater disposal costs. Specifically, we decided to test GZ7-3, which presented the highest selectivity among our membranes. Under this test, the membrane achieved TOC abatement of 95.4

% (Fig. 9a), and ion rejection of 79.0 % (Fig. 9b), bringing down the concentration of organic carbon and the conductivity of the permeate to 26 mg L^{-1} and 99 µS cm^{-1}, respectively. The great selectivity of the GZ7-3 membrane can be ascribed to a combination of the size-sieving and charge exclusion effects, when compared with the bare support, the GZ7-3 membrane showed a strong ability to reduce the absorbance of
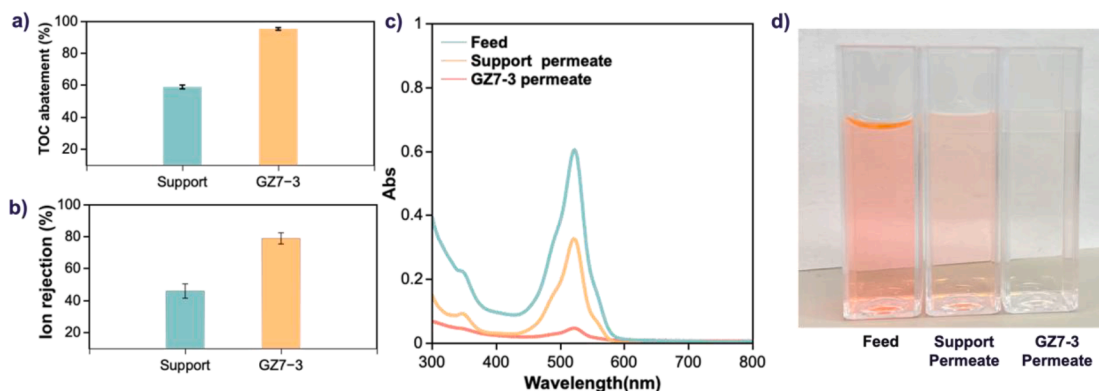

Fig. 9. Filtration of W-IFP: (a) Total organic carbon (TOC) abatement; (b) Ion rejection; (c) UV–Vis spectra of the starting W-IFP (feed) and the permeates after the filtration on the bare support and the GZ7-3 membrane. Error bars indicate the experimental errors in the determination of the TOC and ionic rejections.

the visible light of the effluent. As depicted in Fig. 9c, the intensity of the absorbance peak at 523 nm was reduced by 93 %, yielding a permeate with no relevant absorbance in the visible light range (400–700 nm). Indeed, the final permeate which resulted colorless to the naked eye (Fig. 9d). Therefore, the permeate potentially can be re-used for a new washing cycle after the addition of detergents.

4. Conclusions

In this study, GO/ZIF-8 (GZ) nanocomposite membranes were developed using a simple rubbing method by incorporating an appropriate amount of ZIF-8 into the GO-based active layer. The ZIF-8 nanocomposite membranes showed significantly enhanced water flux and selectivity when compared to our crosslinked GO reference. In this context, we present a simple and scalable method for the coating of GO-based membranes with selectivity and permeability in the nanofiltration range. Our GZ membranes were robust to withstand multiple washing cycles and reusable, as shown in Fig. S5 for a GZ7–3 membrane specimen. The GZ membranes exhibited tremendous potential for various water treatment applications, particularly in the effective removal of micropollutants in a wastewater treatment plant effluent, the abatement of geosmin in RAS water, and the purification of washing water from industrial printing. This work highlights the significant possibilities of the novel GZ composite membranes, which consist of a stable 2D/3D structure, for efficient nanofiltration processes. Furthermore, this study provides new opportunities for developing high-performance, stable, and antifouling composite GO-based membranes, which can be applied across various industries.

CRediT authorship contribution statement

Xinxin Chen: Writing – original draft, Methodology, Investigation, Formal analysis, Data curation, Conceptualization. **Vittorio Boffa:** Writing – review & editing, Supervision, Project administration, Funding acquisition, Data curation, Conceptualization. **Elisa Gaggero:** Methodology, Investigation, Formal analysis. **Fanpeng Meng:** Writing – review & editing, Resources, Investigation, Data curation. **Riccardo Navone:** Writing – review & editing, Resources, Methodology, Data curation. **Daming Sun:** Methodology, Investigation, Formal analysis. **Paola Calza:** Writing – review & editing, Supervision, Methodology, Funding acquisition, Data curation. **Murat Nulati Yesibolati:** Writing – review & editing, Investigation, Data curation. **Peter Kjær Kristensen:** Methodology, Investigation. **Yuanzheng Yue:** Writing – review & editing, Supervision, Methodology, Funding acquisition, Data curation.

Declaration of competing interest

The authors declare that they have no known competing financial interests or personal relationships that could have appeared to influence the work reported in this paper.

Data availability

Data will be made available on request.

Appendix A. Supplementary data

Supplementary data to this article can be found online at https://doi. org/10.1016/j.cej.2024.150207.

References

[1] N. Akhtar, M.I. Syakir Ishak, S.A. Bhawani, K. Umar, Various natural and anthropogenic factors responsible for water quality degradation: a review, Water 13 (2021) 2660, https://doi.org/10.3390/w13192660.
[2] R. Singh, N. Hankins, Emerging membrane Technology for Sustainable Water Treatment, Elsevier, 2016.
[3] M. Issaoui, S. Jellali, A.A. Zorpas, P. Dutournie, Membrane technology for sustainable water resources management: challenges and future projections, Sustain. Chem. Pharm. 25 (2022) 100590, https://doi.org/10.1016/j.scp.2021.100590.
[4] A. Popova, R. Rattanakom, Z.-Q. Yu, Z. Li, K. Nakagawa, T. Fujioka, Evaluating the potential of nanofiltration membranes for removing ammonium, nitrate, and nitrite in drinking water sources, Water Res. (2023) 120484, https://doi.org/10.1016/j.watres.2023.120484.
[5] D. Yu, X. Xiao, C. Shokoohi, Y. Wang, L. Sun, Z. Juan, M.J. Kipper, J. Tang, L. Huang, G.S. Han, H.S. Jung, J. Chen, Recent advances in stimuli-responsive smart membranes for nanofiltration, Adv. Funct. Mater. 33 (2023) 2211983, https://doi.org/10.1002/adfm.202211983.
[6] X. Ma, C.A. Quist-Jensen, A. Ali, V. Boffa, Desalination of groundwater from a well in Puglia region (Italy) by Al2O3-doped silica and polymeric nanofiltration membranes, Nanomaterials 10 (2020) 1738, https://doi.org/10.3390/nano10091738.
[7] N. Meftah, A. Ezzeddine, A. Bedoui, A. Hannachi, Nanofiltration polishing membrane process for fluoride removal, DESALINATION WATER Treat. 198 (2020) 90–97, https://doi.org/10.5004/dwt.2020.26029.
[8] W. Song, L.Y. Lee, E. Liu, X. Shi, S.L. Ong, H.Y. Ng, Spatial variation of fouling behavior in high recovery nanofiltration for industrial reverse osmosis brine treatment towards zero liquid discharge, J. Membr. Sci. 609 (2020) 118185, https://doi.org/10.1016/j.memsci.2020.118185.
[9] Y. Ji, W. Qian, Y. Yu, Q. An, L. Liu, Y. Zhou, C. Gao, Recent developments in nanofiltration membranes based on nanomaterials, Chin. J. Chem. Eng. 25 (2017) 1639–1652, https://doi.org/10.1016/j.cjche.2017.04.014.
[10] (n.d.) (2023) accessed August 15, https://pubs.acs.org/doi/full/10.1021/nn4055682.
[11] L. Yang, X. Xiao, S. Shen, J. Lama, M. Hu, F. Jia, Z. Han, H. Qu, L. Huang, Y. Wang, T. Wang, Z. Ye, Z. Zhu, J. Tang, J. Chen, Recent advances in graphene oxide membranes for nanofiltration, ACS Appl. Nano Mater. 5 (2022) 3121–3145, https://doi.org/10.1021/acsanm.1c04469.
[12] W. Jin, Graphene-Based Membranes for Nanofiltration, in: Nanofiltration, John Wiley & Sons, Ltd, 2021: pp. 1125–1164. https://doi.org/10.1002/9783527824984.ch26.
[13] R. Cruz-Silva, M. Endo, M. Terrones, Graphene oxide films, fibers, and membranes, Nanotechnol. Rev. 5 (2016) 377–391, https://doi.org/10.1515/ntrev-2015-0041.
[14] H.M. Hegab, L. Zou, Graphene oxide-assisted membranes: fabrication and potential applications in desalination and water purification, J. Membr. Sci. 484 (2015) 95–106, https://doi.org/10.1016/j.memsci.2015.03.011.
[15] J. Liu, S. Wang, R. Yang, L. Li, S. Liang, L. Chen, Bio-inspired graphene oxide-amino acid cross-linked framework membrane trigger high water permeance and high metal ions rejection, J. Membr. Sci. 659 (2022) 120745, https://doi.org/10.1016/j.memsci.2022.120745.
[16] Z. Han, X. Xiao, H. Qu, M. Hu, C. Au, A. Nashalian, X. Xiao, Y. Wang, L. Yang, F. Jia, T. Wang, Z. Ye, P. Servati, L. Huang, Z. Zhu, J. Tang, J. Chen, Ultrafast and selective nanofiltration enabled by graphene oxide membranes with unzipped carbon nanotube networks, ACS Appl. Mater. Interfaces 14 (2022) 1850–1860, https://doi.org/10.1021/acsami.1c17201.
[17] Z. Zhang, X. Xiao, Y. Zhou, L. Huang, Y. Wang, Q. Rong, Z. Han, H. Qu, Z. Zhu, S. Xu, J. Tang, J. Chen, Bioinspired graphene oxide membranes with pH-responsive nanochannels for high-performance nanofiltration, ACS Nano 15 (2021) 13178–13187, https://doi.org/10.1021/acsnano.1c02719.
[18] C.-N. Yeh, K. Raidongia, J. Shao, Q.-H. Yang, J. Huang, On the origin of the stability of graphene oxide membranes in water, Nat. Chem. 7 (2015) 166–170, https://doi.org/10.1038/nchem.2145.
[19] S. Sharif, K.S. Ahmad, F. Rehman, Z. Bhatti, K.H. Thebo, Two-dimensional graphene oxide based membranes for ionic and molecular separation: current status and challenges, J. Environ. Chem. Eng. 9 (2021) 105605, https://doi.org/10.1016/j.jece.2021.105605.
[20] S. Begum, Z. Hassan, S. Bräse, C. Wöll, M. Tsotsalas, Metal-organic framework-templated biomaterials: recent Progress in synthesis, functionalization, and applications, Acc. Chem. Res. 52 (2019) 1598–1610, https://doi.org/10.1021/acs.accounts.9b00039.
[21] R. Zou, A.I. Abdel-Fattah, H. Xu, Y. Zhao, D.D. Hickmott, Storage and separation applications of nanoporous metal–organic frameworks, CrystEngComm 12 (2010) 1337–1353, https://doi.org/10.1039/B909643B.
[22] X. Chen, V. Boffa, X. Ma, G. Magnacca, P. Calza, D. Wang, F. Meng, A.H. Nielsen, F. Deganello, K. Li, Y. Yue, Zeolite imidazolate Frameworks-8@SiO2–ZrO2 crystal-amorphous hybrid Core-Shell structure as a building block for water purification membranes, ACS Appl. Mater. Interfaces 16 (2024) 11835–11848, https://doi.org/10.1021/acsami.3c19559.
[23] M. Dahanayaka, R. Babicheva, Z. Chen, A.-W.-K. Law, M.S. Wu, K. Zhou, Atomistic simulation study of GO/HKUST-1 MOF membranes for seawater desalination via pervaporation, Appl. Surf. Sci. 503 (2020) 144198, https://doi.org/10.1016/j.apsusc.2019.144198.

[24] X. Sui, H. Ding, Z. Yuan, C.F. Leong, K. Goh, W. Li, N. Yang, D.M. D'Alessandro, Y. Chen, The roles of metal-organic frameworks in modulating water permeability of graphene oxide-based carbon membranes, Carbon 148 (2019) 277–289, https://doi.org/10.1016/j.carbon.2019.03.049.

[25] H. Qu, X. Xiao, Z. Han, M. Hu, S. Shen, L. Yang, F. Jia, T. Wang, Z. Ye, W. Sun, Y. Wang, L. Huang, Z. Zhu, P. Servati, J. Tang, J. Chen, Graphene oxide nanofiltration membrane based on three-dimensional size-controllable metal-organic frameworks for water treatment, ACS Appl. Nano Mater. 5 (2022) 5196–5207, https://doi.org/10.1021/acsanm.2c00234.

[26] R. Zhang, J. Cao, Y. Liu, J. Guan, M. He, Z. Jiang, Metal-organic framework-intercalated graphene oxide membranes for highly efficient oil/water separation, Ind. Eng. Chem. Res 59 (2020) 16762–16771, https://doi.org/10.1021/acs.iecr.0c02721.

[27] R. Heu, M. Ateia, C. Yoshimura, Photocatalytic nanofiltration membrane using zr-MOF/GO nanocomposite with high-flux and anti-fouling properties, Catalysts 10 (2020) 711, https://doi.org/10.3390/catal10060711.

[28] R. Chang, S. Ma, X. Guo, J. Xu, C. Zhong, R. Huang, J. Ma, Hierarchically assembled graphene oxide composite membrane with self-healing and high-efficiency water purification performance, ACS Appl. Mater. Interfaces 11 (2019) 46251–46260, https://doi.org/10.1021/acsami.9b18018.

[29] X. Yan, Y. Wang, Z. Huang, Z. Gao, X. Mao, M.J. Kipper, L. Huang, J. Tang, Janus polyacrylonitrile/carbon nanotube nanofiber membranes for oil/water separation, ACS Appl. Nano Mater. 6 (2023) 4511–4521, https://doi.org/10.1021/acsanm.3c00006.

[30] Y. Li, L.H. Wee, A. Volodin, J.A. Martens, I.F.J. Vankelecom, Polymer supported ZIF-8 membranes prepared via an interfacial synthesis method, Chem. Commun. 51 (2015) 918–920, https://doi.org/10.1039/C4CC06699E.

[31] G. Liu, W. Jin, N. Xu, Graphene-based membranes, Chem. Soc. Rev. 44 (2015) 5016–5030, https://doi.org/10.1039/C4CS00423J.

[32] A. Suri, L. Calzavarini, A.B. Strunck, G. Magnacca, V. Boffa, Comparison of chemical cross-linkers with branched and linear molecular structures for stabilization of graphene oxide membranes and their performance in ethanol dehydration, Ind. Eng. Chem. Res. 58 (2019) 18788–18797, https://doi.org/10.1021/acs.iecr.9b01532.

[33] V. Boffa, H. Etmimi, P.E. Mallon, H.Z. Tao, G. Magnacca, Y.Z. Yue, Carbon-based building blocks for alcohol dehydration membranes with disorder-enhanced water permeability, Carbon 118 (2017) 458–466, https://doi.org/10.1016/j.carbon.2017.03.077.

[34] S.R. Venna, J.B. Jasinski, M.A. Carreon, Structural evolution of zeolitic imidazolate framework-8, J. Am. Chem. Soc. 132 (2010) 18030–18033, https://doi.org/10.1021/ja109268m.

[35] X. Ma, K. Janowska, V. Boffa, D. Fabbri, G. Magnacca, P. Calza, Y. Yue, Surfactant-assisted fabrication of alumina-doped amorphous silica nanofiltration membranes with enhanced water purification performances, Nanomaterials 9 (2019) 1368, https://doi.org/10.3390/nano9101368.

[36] E. Gaggero, M.J. López-Muñoz, M.C. Paganini, A. Arencibia, S. Bertinetti, N. Fernández de Paz, P. Calza, Mercury and organic pollutants removal from aqueous solutions by heterogeneous photocatalysis with ZnO-based materials, Molecules 28 (2023) 2650, https://doi.org/10.3390/molecules28062650.

[37] X. Wang, B. Li, T. Zhang, X. Li, Performance of nanofiltration membrane in rejecting trace organic compounds: experiment and model prediction, Desalination 370 (2015) 7–16, https://doi.org/10.1016/j.desal.2015.05.010.

[38] (n.d.) (2023) accessed August 10, https://awwa.onlinelibrary.wiley.com/doi/10.1002/aws2.1289.

[39] Y. Sheng, X. Tang, E. Peng, J. Xue, Graphene oxide based fluorescent nanocomposites for cellular imaging, J. Mater. Chem. B 1 (2012) 512–521, https://doi.org/10.1039/C2TB00123C.

[40] L. Dong, M. Chen, J. Li, D. Shi, W. Dong, X. Li, Y. Bai, Metal-organic framework-graphene oxide composites: a facile method to highly improve the CO2 separation performance of mixed matrix membranes, J. Membr. Sci. 520 (2016) 801–811, https://doi.org/10.1016/j.memsci.2016.08.043.

[41] L. Yang, B. Tang, P. Wu, Metal–organic framework–graphene oxide composites: a facile method to highly improve the proton conductivity of PEMs operated under low humidity, J. Mater. Chem. A 3 (2015) 15838–15842, https://doi.org/10.1039/C5TA03507D.

[42] D. Huang, Q. Xin, Y. Ni, Y. Shuai, S. Wang, Y. Li, H. Ye, L. Lin, X. Ding, Y. Zhang, Synergistic effects of zeolite imidazole FRAMEWORK@GRAPHENE oxide composites in humidified mixed matrix membranes on CO2 separation, RSC Adv. 8 (2018) 6099–6109, https://doi.org/10.1039/C7RA09794H.

[43] X. Wu, H. Zhang, Z. Yin, Y. Yang, Z. Wang, ZIF-8/GO sandwich composite membranes through a precursor conversion strategy for H2/CO2 separation, J. Membr. Sci. 647 (2022) 120291, https://doi.org/10.1016/j.memsci.2022.120291.

[44] F. Jia, L. Yang, L. Sun, D. Yu, Y. Song, Y. Wang, M.J. Kipper, J. Tang, L. Huang, Efficient separation of dyes using two-dimensional heterogeneous composite membranes, Water Res. (2023) 120693, https://doi.org/10.1016/j.watres.2023.120693.

[45] T. Aytug, M.S. Rager, W. Higgins, F.G. Brown, G.M. Veith, C.M. Rouleau, H. Wang, Z.D. Hood, S.M. Mahurin, R.T. Mayes, P.C. Joshi, T. Kuruganti, Vacuum-assisted low-temperature synthesis of reduced graphene oxide thin-film electrodes for high-performance transparent and flexible all-solid-state supercapacitors, ACS Appl. Mater. Interfaces 10 (2018) 11008–11017, https://doi.org/10.1021/acsami.8b01938.

[46] Y. Li, X. Zhang, A. Yang, C. Jiang, G. Zhang, J. Mao, Q. Meng, Polyphenol etched ZIF-8 modified graphene oxide nanofiltration membrane for efficient removal of salts and organic molecules, J. Membr. Sci. 635 (2021) 119521, https://doi.org/10.1016/j.memsci.2021.119521.

[47] S. Abdikheibari, W. Lei, L.F. Dumée, N. Milne, K. Baskaran, Thin film nanocomposite nanofiltration membranes from amine functionalized-boron nitride/polypiperazine amide with enhanced flux and fouling resistance, J. Mater. Chem. A 6 (2018) 12066–12081, https://doi.org/10.1039/C8TA03446J.

[48] V. Nayak, J. Mannekote Shivanna, S. Ramu, S. Radoor, R.G. Balakrishna, Efficacy of electrospun nanofiber membranes on fouling mitigation, A Review, ACS Omega 7 (2022) 43346–43363, https://doi.org/10.1021/acsomega.2c02081.

[49] K. Zhang, R.P. Lively, C. Zhang, R.R. Chance, W.J. Koros, D.S. Sholl, S. Nair, Exploring the framework hydrophobicity and flexibility of ZIF-8: from biofuel recovery to hydrocarbon separations, J. Phys. Chem. Lett. 4 (2013) 3618–3622, https://doi.org/10.1021/jz402019d.

[50] N. Shardt, J.A.W. Elliott, Gibbsian thermodynamics of Wenzel wetting (was Wenzel wrong? revisited), Langmuir 36 (2020) 435–446, https://doi.org/10.1021/acs.langmuir.9b02984.

[51] H. Zhang, Q. He, J. Luo, Y. Wan, S.B. Darling, Sharpening nanofiltration: strategies for enhanced membrane selectivity, ACS Appl. Mater. Interfaces 12 (2020) 39948–39966, https://doi.org/10.1021/acsami.0c11136.

[52] D. Li, M.B. Müller, S. Gilje, R.B. Kaner, G.G. Wallace, Processable aqueous dispersions of graphene nanosheets, Nat. Nanotechnol. 3 (2008) 101–105, https://doi.org/10.1038/nnano.2007.451.

[53] F. Baskoro, C.-B. Wong, S.R. Kumar, C.-W. Chang, C.-H. Chen, D.W. Chen, S.J. Lue, Graphene oxide-cation interaction: inter-layer spacing and zeta potential changes in response to various salt solutions, J. Membr. Sci. 554 (2018) 253–263, https://doi.org/10.1016/j.memsci.2018.03.006.

[54] Z. Latrach, E. Moumen, S. Kounbach, S. El Hankari, Mixed-ligand strategy for the creation of hierarchical porous ZIF-8 for enhanced adsorption of copper ions, ACS Omega 7 (2022) 15862–15869, https://doi.org/10.1021/acsomega.2c00980.

[55] M.R. bin Shaharudin, C.D. Williams, A. Achari, R.R. Nair, P. Carbone, Decoding the interplay between topology and surface charge in graphene oxide membranes during humidity induced swelling, ACS Nano 17 (2023) 21923–21934, https://doi.org/10.1021/acsnano.3c08260.

[56] F. Fei, L. Cseri, G. Szekely, C.F. Blanford, Robust covalently cross-linked polybenzimidazole/graphene oxide membranes for high-flux organic solvent nanofiltration, ACS Appl. Mater. Interfaces 10 (2018) 16140–16147, https://doi.org/10.1021/acsami.8b03591.

[57] W.-S. Hung, C.-H. Tsou, M. De Guzman, Q.-F. An, Y.-L. Liu, Y.-M. Zhang, C.-C. Hu, K.-R. Lee, J.-Y. Lai, Cross-linking with diamine monomers to prepare composite graphene oxide-framework membranes with varying d-spacing, Chem. Mater. 26 (2014) 2983–2990, https://doi.org/10.1021/cm5007873.

[58] E.A. Chernova, K.E. Gurianov, D.I. Petukhov, A.P. Chumakov, R.G. Valeev, V.A. Brotsman, A.V. Garshev, A.A. Eliseev, Oxidized carbon-based spacers for pressure-resistant graphene oxide membranes, Membranes 12 (2022) 934, https://doi.org/10.3390/membranes12100934.

[59] R.K. Joshi, P. Carbone, F.C. Wang, V.G. Kravets, Y. Su, I.V. Grigorieva, H.A. Wu, A.K. Geim, R.R. Nair, Precise and ultrafast molecular sieving through graphene oxide membranes, Science 343 (2014) 752–754, https://doi.org/10.1126/science.1245711.

[60] O. Kwon, Y. Choi, E. Choi, M. Kim, Y.C. Woo, D.W. Kim, Fabrication techniques for graphene oxide-based molecular separation membranes: towards industrial application, Nanomaterials 11 (2021) 757, https://doi.org/10.3390/nano11030757.

[61] F. Jia, X. Xiao, A. Nashalian, S. Shen, L. Yang, Z. Han, H. Qu, T. Wang, Z. Ye, Z. Zhu, L. Huang, Y. Wang, J. Tang, J. Chen, Advances in graphene oxide membranes for water treatment, Nano Res. 15 (2022) 6636–6654, https://doi.org/10.1007/s12274-022-4273-y.

[62] Y. Oh, D.L. Armstrong, C. Finnerty, S. Zheng, M. Hu, A. Torrents, B. Mi, Understanding the pH-responsive behavior of graphene oxide membrane in removing ions and organic micropollutants, J. Membr. Sci. 541 (2017) 235–243, https://doi.org/10.1016/j.memsci.2017.07.005.

[63] A. Morelos-Gomez, R. Cruz-Silva, H. Muramatsu, J. Ortiz-Medina, T. Araki, T. Fukuyo, S. Tejima, K. Takeuchi, T. Hayashi, M. Terrones, M. Endo, Effective NaCl and dye rejection of hybrid graphene oxide/graphene layered membranes, Nat. Nanotechnol. 12 (2017) 1083–1088, https://doi.org/10.1038/nnano.2017.160.

[64] M. Hu, B. Mi, Enabling graphene oxide nanosheets as water separation membranes, Environ. Sci. Technol. 47 (2013) 3715–3723, https://doi.org/10.1021/es400571g.

[65] W.-H. Zhang, M.-J. Yin, C.-G. Jin, Z.-J. Liu, N. Wang, Q.-F. An, Ice-crystal templating approach for tailoring mass transfer channels in graphene oxide membranes for high-performance dye/salt separation, Carbon 183 (2021) 119–127, https://doi.org/10.1016/j.carbon.2021.06.077.

[66] W. Choi, J. Choi, J. Bang, J.-H. Lee, Layer-by-layer assembly of graphene oxide nanosheets on polyamide membranes for durable reverse-osmosis applications, ACS Appl. Mater. Interfaces 5 (2013) 12510–12519, https://doi.org/10.1021/am403790s.

[67] S. Cong, Y. Yuan, J. Wang, Z. Wang, F. Kapteijn, X. Liu, Highly water-permeable metal-organic framework MOF-303 membranes for desalination, J. Am. Chem. Soc. 143 (2021) 20055–20058, https://doi.org/10.1021/jacs.1c10192.

[68] Y. Xiao, W. Zhang, Y. Jiao, Y. Xu, H. Lin, Metal-phenolic network as precursor for fabrication of metal-organic framework (MOF) nanofiltration membrane for efficient desalination, J. Membr. Sci. 624 (2021) 119101, https://doi.org/10.1016/j.memsci.2021.119101.

[69] X. Liu, N.K. Demir, Z. Wu, K. Li, Highly water-stable zirconium metal-organic framework UiO-66 membranes supported on alumina hollow fibers for

desalination, J. Am. Chem. Soc. 137 (2015) 6999–7002, https://doi.org/10.1021/jacs.5b02276.

[70] M. Jian, R. Qiu, Y. Xia, J. Lu, Y. Chen, Q. Gu, R. Liu, C. Hu, J. Qu, H. Wang, X. Zhang, Ultrathin water-stable metal-organic framework membranes for ion separation, Sci. Adv. 6 (2020) eaay3998, https://doi.org/10.1126/sciadv.aay3998.

[71] L. Yang, Z. Wang, J. Zhang, Zeolite imidazolate framework hybrid nanofiltration (NF) membranes with enhanced permselectivity for dye removal, J. Membr. Sci. 532 (2017) 76–86, https://doi.org/10.1016/j.memsci.2017.03.014.

[72] C. Liu, L. Shi, R. Wang, Crosslinked layer-by-layer polyelectrolyte nanofiltration hollow fiber membrane for low-pressure water softening with the presence of SO_4^{2-} in feed water, J. Membr. Sci. 486 (2015) 169–176, https://doi.org/10.1016/j.memsci.2015.03.050.

[73] V. Freger, J. Gilron, S. Belfer, TFC polyamide membranes modified by grafting of hydrophilic polymers: an FT-IR/AFM/TEM study, J. Membr. Sci. 209 (2002) 283–292, https://doi.org/10.1016/S0376-7388(02)00356-3.

[74] C. Boo, Y. Wang, I. Zucker, Y. Choo, C.O. Osuji, M. Elimelech, High performance nanofiltration membrane for effective removal of perfluoroalkyl substances at high water recovery, Environ. Sci. Technol. 52 (2018) 7279–7288, https://doi.org/10.1021/acs.est.8b01040.

[75] Q. Sui, X. Cao, S. Lu, W. Zhao, Z. Qiu, G. Yu, Occurrence, sources and fate of pharmaceuticals and personal care products in the groundwater: a review, Emerg. Contam. 1 (2015) 14–24, https://doi.org/10.1016/j.emcon.2015.07.001.

[76] X. Hu, Y. Yu, S. Ren, N. Lin, Y. Wang, J. Zhou, Highly efficient removal of phenol from aqueous solutions using graphene oxide/Al₂O₃ composite membrane,

[77] S. Azaria, J. van Rijn, Off-flavor compounds in recirculating aquaculture systems (RAS): production and removal processes, Aquac. Eng. 83 (2018) 57–64, https://doi.org/10.1016/j.aquaeng.2018.09.004.

[78] F. Jüttner, S.B. Watson, Biochemical and ecological control of geosmin and 2-methylisoborneol in source waters, Appl. Environ. Microbiol. 73 (2007) 4395–4406, https://doi.org/10.1128/AEM.02250-06.

[79] V. Boffa, D. Fabbri, P. Calza, D. Revelli, P.V. Christensen, Potential of nanofiltration technology in recirculating aquaculture systems in a context of circular economy, Chem. Eng. J. Adv. 10 (2022) 100269, https://doi.org/10.1016/j.ceja.2022.100269.

[80] H. Li, Y. Chen, J. Zhang, B. Dong, Pilot study on nanofiltration membrane in advanced treatment of drinking water, Water Supply 20 (2020) 2043–2053, https://doi.org/10.2166/ws.2020.089.

[81] M.B. Dixon, C. Falconet, L. Ho, C.W.K. Chow, B.K. O'Neill, G. Newcombe, Removal of cyanobacterial metabolites by nanofiltration from two treated waters, J. Hazard. Mater. 188 (2011) 288–295, https://doi.org/10.1016/j.jhazmat.2011.01.111.

[82] Y. Chung, M.-Y. Lee, H. Park, Y.-I. Park, S.-E. Nam, P.S. Lee, Y.S. Hwang, S. Kang, Novel preparation of ceramic nanofiltration membrane for the removal of trace organic compounds, Desalination Water Treat. 101 (2018) 31–36, https://doi.org/10.5004/dwt.2018.21642.

J. Porous Mater. 25 (2018) 719–726, https://doi.org/10.1007/s10934-017-0485-z.